ISET Journal of Earthquake Technology, Paper No. 441, Vol. 41, No. 1, March 2004, pp. 75-99

EQUIVALENT ELASTIC MODELING FOR THE DIRECT-DISPLACEMENT-BASED SEISMIC DESIGN OF WOOD STRUCTURES

Andre Filiatrault*, Mary Epperson** and Bryan Folz***
*Professor
Department of Civil, Structural and Environmental Engineering
University at Buffalo
State University of New York
Buffalo, NY 14260, U.S.A.
**Graduate Student Researcher
Department of Structural Engineering
University of California, San Diego, La Jolla
CA 92093, U.S.A.
***Faculty of Civil and Structural Engineering Technology
British Columbia Institute of Technology
3700 Willingdon Avenue, Burnaby
B.C., Canada V5G-3H2

ABSTRACT

Direct-displacement seismic design assumes that the response of a structural system can be obtained through a single-degree-of-freedom (SDOF) model with equivalent elastic lateral stiffness and viscous damping properties representative of the characteristics of the structure at a target displacement. To date, this assumption has not been validated for structures exhibiting highly pinched hysteretic response, as is typical of wood structures. This paper presents and discusses the results of an extensive numerical investigation aimed at assessing the equivalent linear modeling of light-frame wood buildings. The findings from this study indicate that elastic models, based on equivalent viscous damping representative of first cycle hysteretic response, with no pinching behavior, under-predict by 20% on average the seismic response of fully non-linear models. On the other hand, elastic models, based on equivalent viscous damping representative of hysteretic cyclic response past the first (virgin) cycle, with pinching behavior present, over-predict significantly (40% on average) the seismic response of fully non-linear models. Various approaches are briefly presented to show how the response differences between equivalent linear elastic and fully inelastic building models can be taken into account in the direct-displacement based seismic design procedure for light-frame wood buildings.

KEYWORDS: Direct-Displacement, Earthquakes, Performance-Based, Seismic, Wood

INTRODUCTION

Performance-based seismic design of structures is based on coupling multiple performance limit states with specified seismic hazard levels. This design philosophy overcomes several of the shortcomings of the traditional force-based seismic design procedure, which has been the cornerstone of building code requirements to date. Although the performance-based seismic design approach has advanced for some types of structures, such as reinforced concrete buildings and bridges, to the point where it may be ready for incorporation into future generations of building and bridge codes, its application to light-frame wood buildings has only recently been formulated (Filiatrault and Folz, 2002).

Since inter-story drift is a key parameter for the control of damage in wood buildings (Porter et al., 2001), it is rational to examine a performance-based seismic design procedure, wherein displacements are at the core of the design process. In this regard, the direct-displacement approach, proposed by Priestley (1993, 1998) for reinforced concrete structures, is an attractive seismic design procedure to adopt for wood buildings.

Direct-displacement seismic design assumes that the structural system can be represented by a single-degree-of-freedom (SDOF) model with equivalent elastic lateral stiffness, k_{eq}, and viscous damping ratio, ζ_{eq}, representative of the characteristics of the original structure at a target displacement, Δ_t. This

assumption is commonly used for systems exhibiting fully developed hysteretic behaviour, such as reinforced concrete structures, but has not yet been completely validated for wood structures that may exhibit highly pinched hysteretic response. Figure 1 shows the hysteretic response typically displayed by light-framed wood buildings. It is observed from this figure that the structure develops significant pinching in the force-displacement response after the first (virgin) cycle of loading. This pinched hysteretic response continues in subsequent cycles that are loaded to the same target displacement, Δ_t, if fatigue under continued loading is not a factor.

The main objective of this paper is to ascertain the validity of the equivalent linear elastic modeling of light-frame wood buildings by comparing the results of non-linear and equivalent linear dynamic analyses for a suite of four prototype index wood buildings.

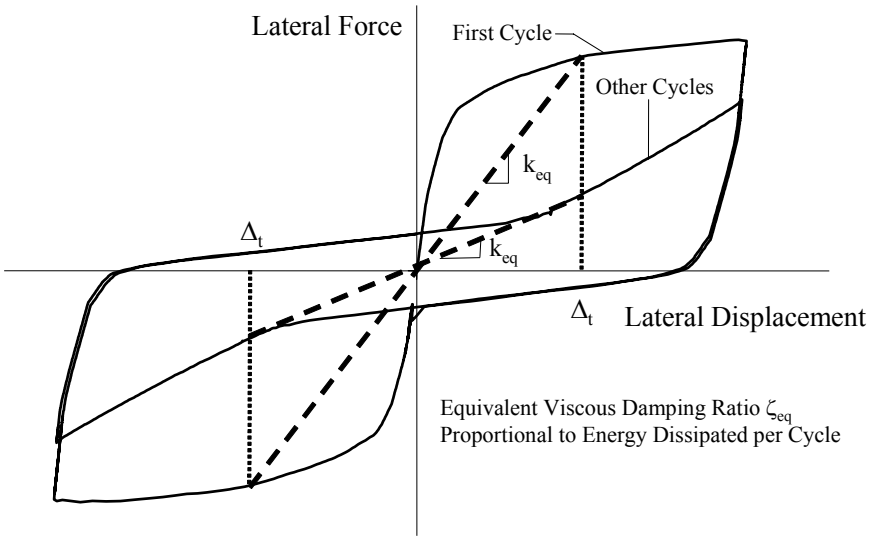

Fig. 1 Equivalent linear elastic modeling of wood structures

OVERVIEW OF DISPLACEMENT-BASED SEISMIC DESIGN PROCEDURE

The basic elements of the displacement-based seismic design procedure for light-frame wood buildings are briefly summarized in this section. A more detailed presentation of this design approach has been provided previously by Filiatrault and Folz (2002).

The central concept of the direct-displacement method, as originally proposed by Priestley (1993, 1998), is that the seismic design of a structure is based on a specified target displacement for a given seismic hazard level. For this purpose, the structure is modeled as a single-degree-of-freedom (SDOF) system with equivalent elastic lateral stiffness and viscous damping properties representative of the global behavior of the actual structure at the target displacement.

The first step in this design procedure is the definition of the target displacement Δ_t that the building should not exceed under a given seismic hazard level. The seismic hazard associated with the target displacement must then be defined in terms of a design relative displacement response spectrum corresponding to the equivalent viscous damping exhibited by the structure at the target displacement.

Once the design performance level and associated seismic hazard have been defined, a structural lateral load-resisting system must be specified for subsequent performance evaluation. Most light-frame wood buildings in North America use wood shear wall assemblies as the primary lateral load-resisting structural system. In addition, wall finish materials such as gypsum wallboard and stucco may contribute significantly to the lateral stiffness and strength of wood buildings (Filiatrault et al., 2002).

In order to capture the energy dissipation characteristics of the structure at the target displacement, an equivalent viscous damping ratio must be determined. For this purpose, a damping database must be established for the selected structural system from the global hysteretic behavior of the structure. Note that for wood structures, a nominal damping ratio needs to be added to this hysteretic damping to account for the energy dissipation characteristic of other structural and non-structural elements in the structure (Foliente, 1995). From Figure 1, it is seen that the equivalent viscous damping ratio is dependent upon

whether the first (virgin) or subsequent cycles are used to determine its value. This feature adds complexity to the displacement-based seismic design process and is discussed further in this paper.

Knowing the target displacement and the equivalent viscous damping of the building at the target displacement, the equivalent elastic period of the building, T_{eq}, can be obtained directly from the design displacement response spectrum. With the building represented as an equivalent linear SDOF system, the required equivalent lateral stiffness, k_{eq}^{r}, is given by:

$$k_{eq}^{r} = \frac{4\pi^2 W_{eff}}{g T_{eq}^2} \tag{1}$$

where W_{eff} is the effective seismic weight acting on the building and g is the acceleration of gravity.

Table 1: Construction Details for Index Buildings

Index Building	Components	Construction Details
Small House	Exterior Walls	Stucco (20 mm thick) on outside. Gypsum wallboard (12 mm thick) on inside. Furring nails (9 mm head), spaced at 150 mm on center along vertical studs used to attach wire mesh of stucco finish to wood framing.
	Interior Walls	Gypsum wallboard (12 mm thick) on both sides. Drywall nails (40 mm long) spaced at 175 mm on center along vertical studs (spaced at 400 mm on center) used to attach gypsum walls to framing. Gypsum wallboard panels positioned vertically.
	Floor Diaphragms	Joists (38×139 mm) spaced at 400 mm on center and spanning up to 2.7 m along with solid 25×139 mm diagonal sheathing. Floor supported by 89×139 mm girders sitting on pier blocks.
	Roof Diaphragm	Composite shingle felt and solid 25×139 mm straight sheathing.
	Ceiling	Gypsum wallboard (12 mm thick).
Large House	Exterior Walls	Stucco (20 mm thick) over 11 mm Oriented Strand Board (OSB) on outside. Gypsum wallboard (12 mm thick) on inside. Crown staples (25 mm long) spaced at 150 mm on center along vertical studs used to attach wire mesh of stucco finish to wood framing. Eight-penny common nails spaced at 150, 100 or 75 mm along edges and 150 mm on field used to attach OSB panels to framing.
	Interior Walls	Same as small house.
	Floor Diaphragms	Joists (38×286 mm) spaced at 400 mm on center and spanning up to 2.7 m along with 19 mm tongue and groove plywood sheathing.
	Roof Diaphragm	Composite shingle felt over 11 mm OSB sheathing.
	Ceiling	Gypsum wallboard (12 mm thick).
Small Townhouse	Exterior Walls	Same as large house except furring nails (9.5 mm head) spaced at 150 mm on center along vertical studs used to attach wire mesh of stucco finish to wood framing.
	Interior Walls	Same as small house.
	Floor Diaphragms	Same as large house.
	Roof Diaphragm	Joists (38×139 mm) spaced at 600 mm on center. Plywood (12 mm thick) or OSB (12 mm thick) sheathing.
	Ceiling	Gypsum wallboard (12 mm thick).
Apartment	Exterior Walls	Same as small townhouse.
	Interior Walls	Same as small house.
	Floor Diaphragms	Same as large house.
	Roof Diaphragm	Same as small townhouse.
	Ceiling	Gypsum wallboard (16 mm thick).

The actual equivalent lateral stiffness, k_{eq}^{a}, of the building at the target displacement, Δ_t, can be determined from the results of a static pushover analysis. The actual equivalent lateral stiffness of the building must be compared to the required equivalent lateral stiffness. If these two stiffness values differ substantially, the lateral-load resisting system of the building must be modified. If the actual lateral stiffness of the building is nearly equal to the required lateral stiffness, the design process is completed by computing the required base shear capacity, V_b, of the building:

$$V_b = k_{eq}^{a} \Delta_t \tag{2}$$

This base shear can then be used to design the other elements of the structure.

As presented, this direct-displacement seismic design strategy requires detailed knowledge of the global non-linear monotonic load-displacement behavior (pushover) of the building, as well as the variation of the global equivalent viscous damping with displacement amplitude. These requirements can be considered as a limitation of the direct-displacement seismic design procedure since knowledge of the behavior of light-frame wood construction at the system level is not well established. To obtain this information, further system level testing is required in parallel with the on-going development of specialized numerical models for light-frame wood construction.

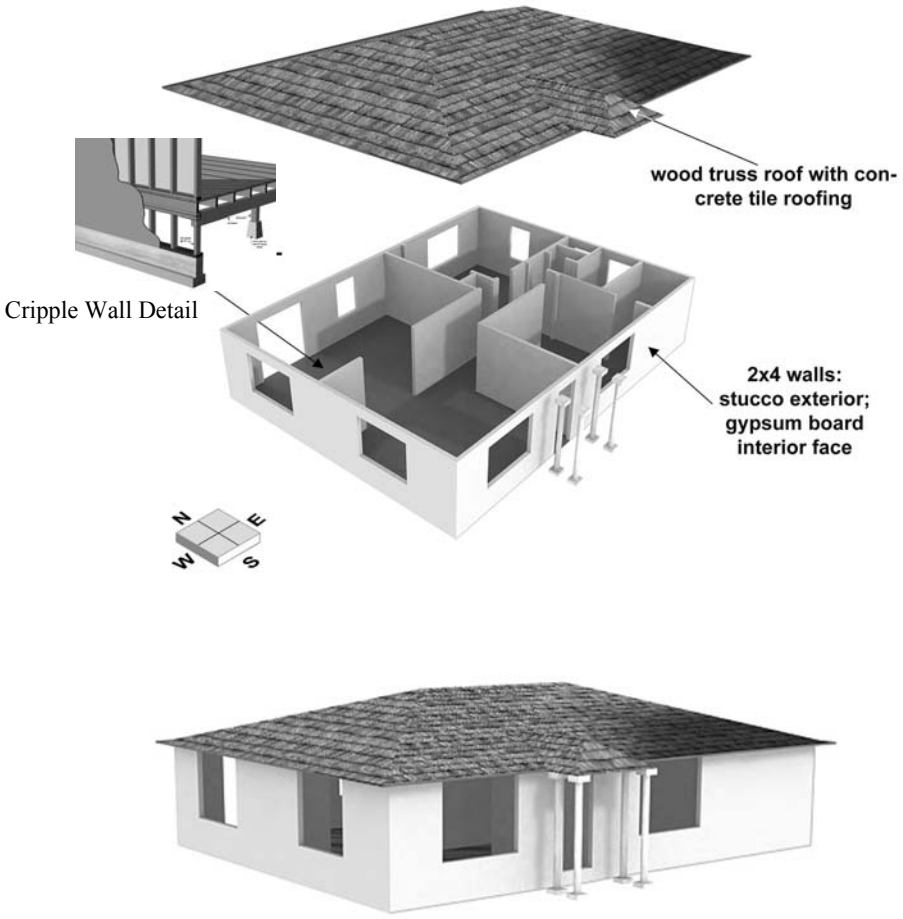

Fig. 2 Small house index building (reproduced, with permission, from Reitherman et al. (2003))

DESCRIPTION OF INDEX WOOD BUILDINGS

In order to assess the equivalent linear elastic modeling for wood buildings, a suite of four different index wood buildings are considered. These prototype index buildings were developed under the CUREE-Caltech Woodframe Project in California for use in loss estimation and benefit-to-cost ratio analysis (Porter et al., 2001). Only a brief description of these building configurations is presented here. A summary of pertinent construction details of each building is given in Table 1. A full description of these index buildings has been presented elsewhere (Isoda et al., 2001; Reitherman et al., 2003).

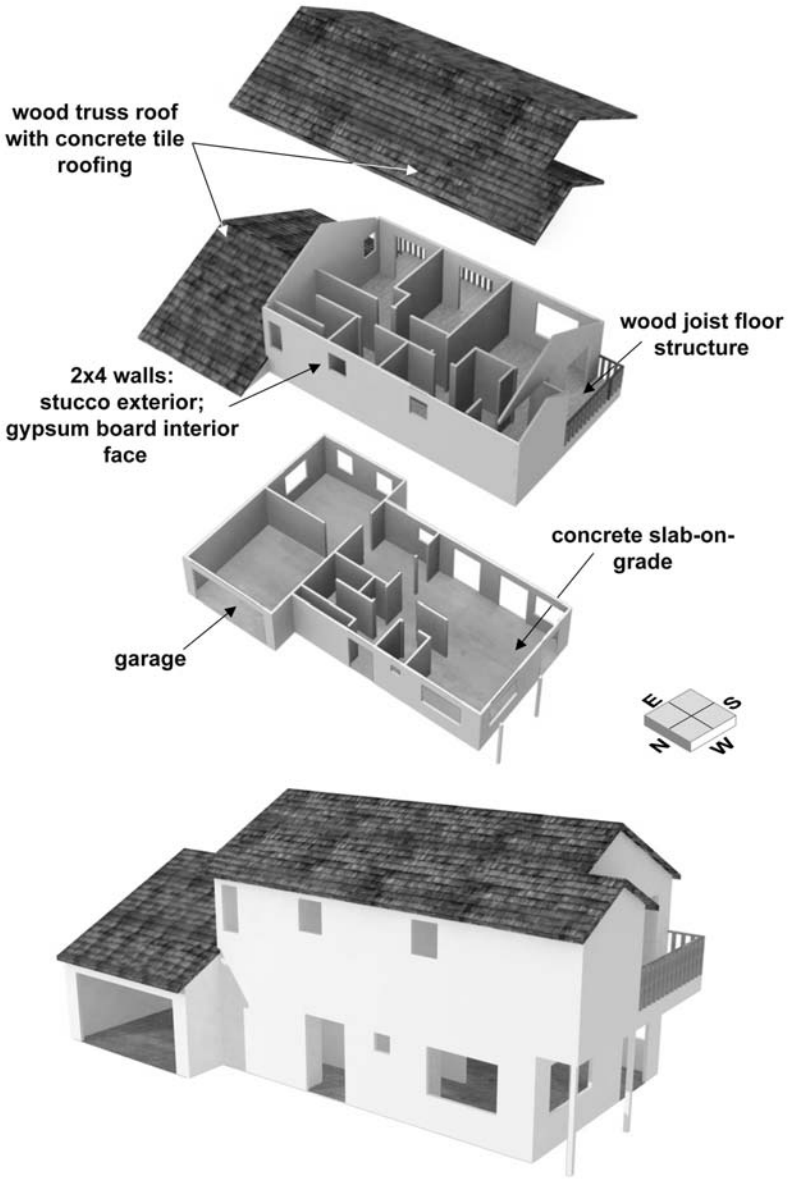

Fig. 3 Large house index building (reproduced, with permission, from Reitherman et al. (2003))

1. Small House

This index building represents a one-story, two-bedroom house built circa 1950 with a simple 110 m^2 floor plan on a level lot, as shown in Figure 2. Prescriptive construction is assumed. The structure is assumed to be founded on wood framed cripple walls, which is typical of construction of this time period in California. The height of the small house from the bottom of the cripple wall to the roof eaves is 3.35 m. Its seismic weight is 205 kN and the initial (elastic) fundamental period is 0.20 s.

This index building was developed to exemplify post-World War II affordable housing that was constructed in large quantities in the United States, either in tracts or one-by-one by small contractors or owner-builders. This was the kind of building that was originally intended for the application of the prescriptive construction provisions included in the Uniform Building Code.

2. Large House

This index building represents an engineered two-story single family dwelling of approximately 225 m^2 on a level lot with a slab-on-grade and spread footings, as shown in Figure 3. This building is assumed to have been built as a housing development "production house" in either the 1980s or 1990s. The height of the large house from the first floor slab to the roof eaves is 5.49 m. Its seismic weight is 305 kN and the initial (elastic) fundamental period is 0.17 s.

This index building was developed to include characteristics encountered in more modern residential construction, such as the higher linear footage of partition walls on the upper floor in the bedrooms and bathrooms than on the ground floor. Also included is the tendency to have much less shear wall in one portion of the ground floor plan in order to accommodate the living room and other common areas.

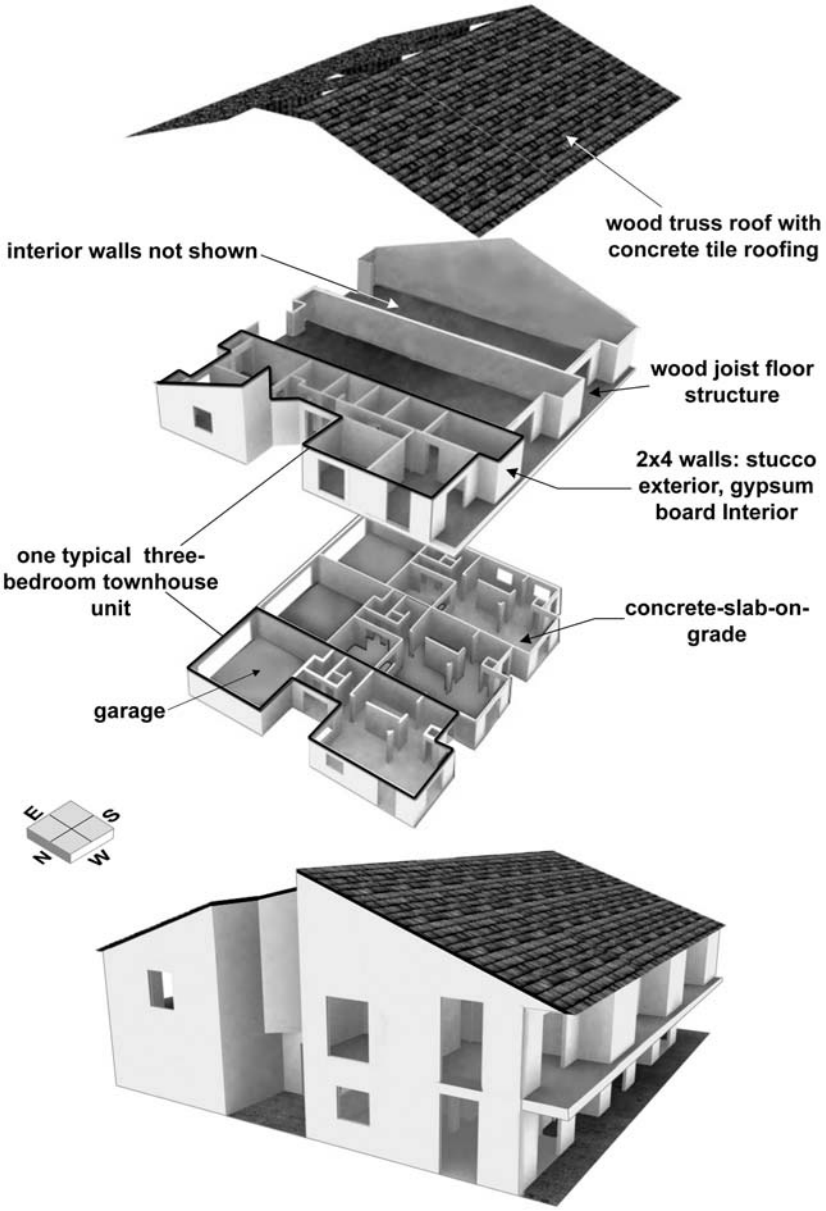

Fig. 4 Townhouse index building (reproduced from, with permission, Reitherman et al. (2003))

3. Small Townhouse

This index building represents a two-story townhouse containing three units, each having approximately 150 m^2 of living space with an attached two-car garage, as shown in Figure 4. It is on a level lot with a slab-on-grade and spread foundations. This building is assumed to have been built as a "production house" in either the 1980s or 1990s, located in either Northern or Southern California. The design is based on engineered construction. The height of the townhouse from the first floor slab to the roof eaves is 5.49 m. Its seismic weight is 840 kN and the initial (elastic) fundamental period is 0.16 s.

Seismically relevant characteristics, that were intentionally featured in this townhouse, include the integral garage and for the end units, the imbalance in plan stiffness between the solid longitudinal wall with gypsum wallboard at the common wall side versus the perforated walls with stucco or OSB on the exterior wall side.

4. Apartment Building

This index building represents a three-story, rectangular apartment with ten units (each with 75 m^2 of living space) and space for mechanical and common areas, as shown in Figure 5. All walls and elevated floors are light wood frame. It has parking on the ground floor. Each unit has two bedrooms and one assigned parking stall. Such buildings were constructed prior to 1970 in Northern or Southern California and "engineered" to a minimal extent. The height of the small townhouse from the first floor slab to the roof eaves is 8.23 m. Its seismic weight is 1550 kN and the initial (elastic) fundamental period is 0.25 s.

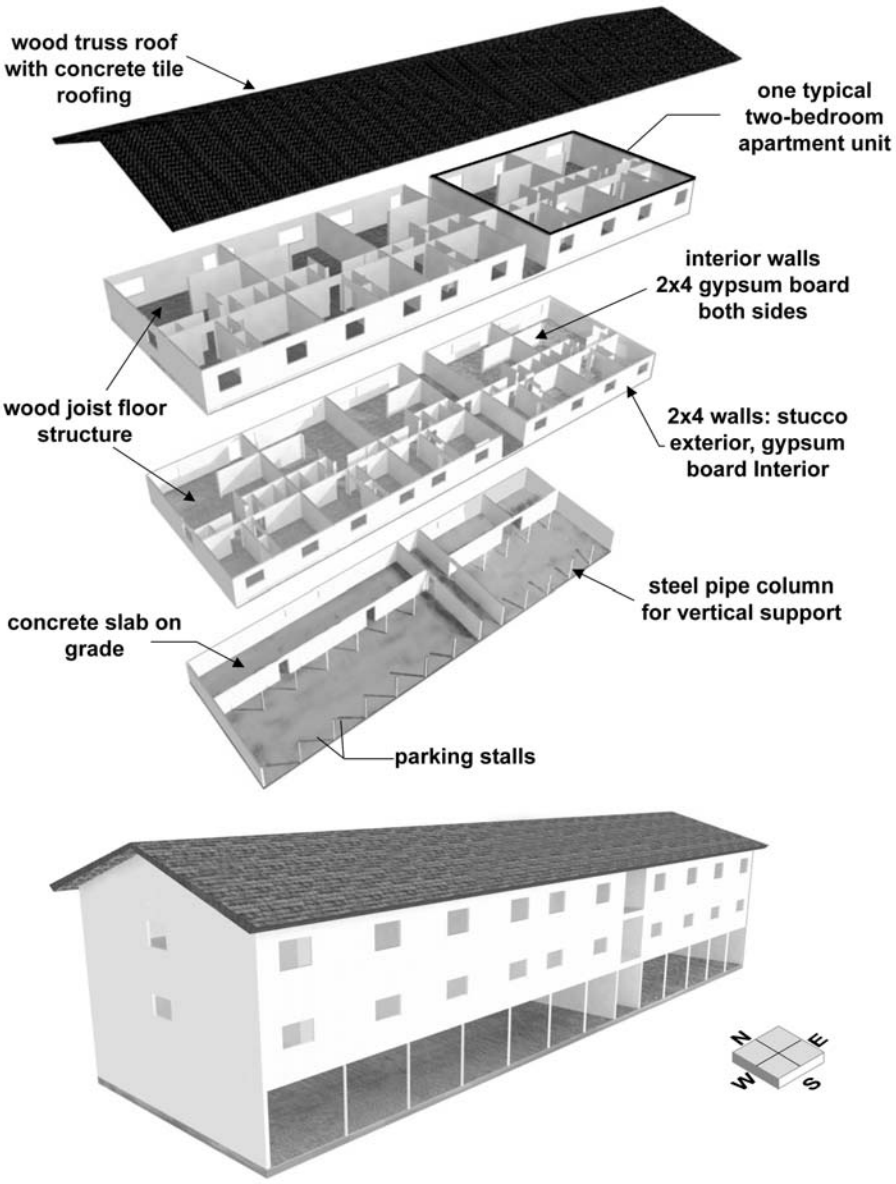

Fig. 5 Apartment index building (reproduced, with permission, from Reitherman et al. (2003))

NUMERICAL MODELING OF INDEX WOOD BUILDINGS

A three-dimensional non-linear seismic analysis of each of the prototype index wood buildings was performed in this study. To complete this task, a 'pancake' modeling approach was adopted (Isoda et al., 2001). This modeling approach simulates the three-dimensional seismic response of a building through a degenerated two-dimensional planar analysis. The inelastic dynamic analysis computer program, RUAUMOKO (Carr, 2000), was used to analyze the pancake model of each index building.

A typical light-frame wood building can be modeled as a planar pancake system with floor and roof diaphragms superimposed on top of each other and inter-connected with zero-height springs representing

wall sections. Figure 6 shows the pancake model corresponding to a simple two-story woodframe building recently tested on a shake table (Isoda et al., 2001; Filiatrault et al., 2002). The lateral load resisting system of this simple test structure is composed of only exterior shear walls. The foundation of the structural model is connected to the floor diaphragm with four zero-height non-linear shear springs representing the four first story shearwalls. Similarly, the floor diaphragm is connected to the roof diaphragm with four additional zero-height non-linear shear springs representing the second story shearwalls. The roof and/or ceiling diaphragm, having high in-plane stiffness in this particular case, is modeled by four plane stress quadrilateral finite elements with very high in-plane stiffness. The floor diaphragm is modeled by plane stress quadrilateral finite elements. The in-plane stiffness of the floor diaphragm can be calibrated to simulate the in-plane response of the floor diaphragm (Isoda et al., 2001).

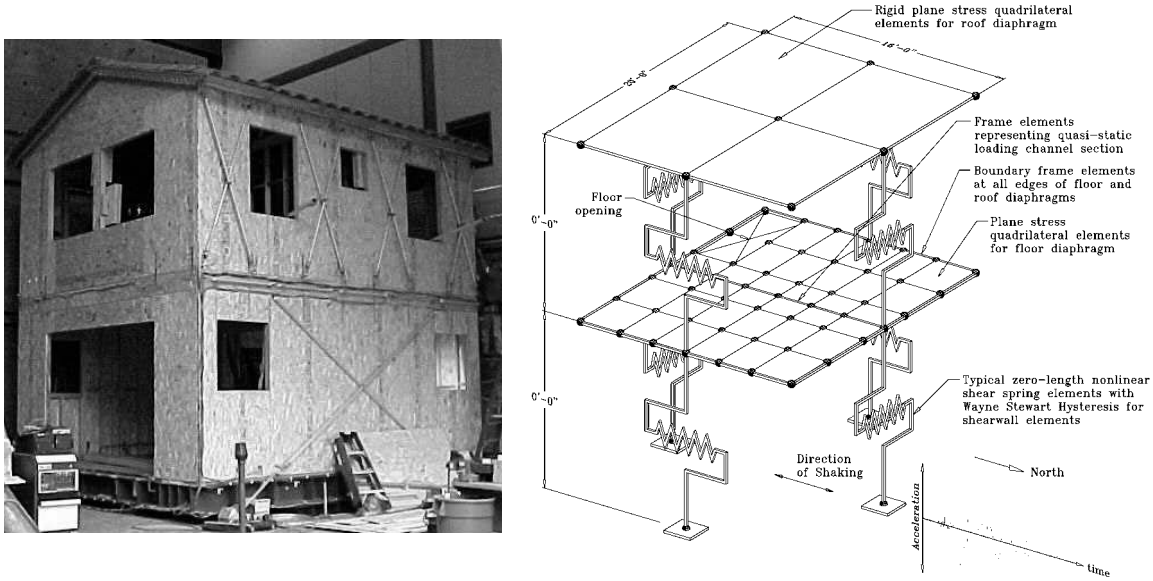

Fig. 6 Two-story woodframe test structure and corresponding pancake model

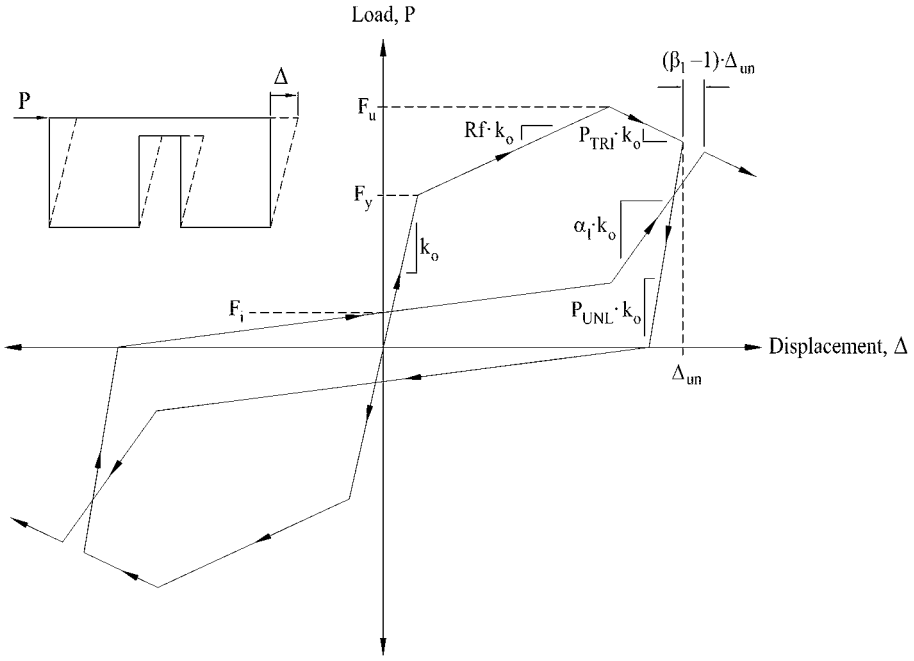

Fig. 7 Wayne Stewart degrading hysteresis rule

Frame elements are used along the four edges of the floor diaphragm to connect the corners of the quadrilateral elements to the shear wall elements. The bending stiffness of the frame elements is assumed very small to allow free deformations of the diaphragm. The axial stiffness of the frame elements is

assumed very high in order to distribute the in-plane forces of the shear elements along the edges of the floor diaphragm.

Each wall in the structure (composed of wood, gypsum and/or stucco) is modeled by a single zero-height non-linear in-plane shear spring using the Wayne Stewart hysteresis rule (Stewart, 1987) shown in Figure 7. This hysteresis rule incorporates stiffness and strength degradation, typical of the racking response of wood, gypsum and stucco walls, and is defined by nine independent physical parameters which are: F_y = Equivalent lateral yield strength; k_o = Initial lateral stiffness; R_f = Post-yield stiffness factor; F_u = Ultimate lateral capacity; F_i = Intercept force; *PTRI* = Tri-linear stiffness factor beyond the ultimate capacity; *PUNL* = Unloading stiffness factor; β_1 = Softening factor; and α_1 = Reloading stiffness factor. The proper evaluation of these hysteretic parameters, for each non-linear shear spring element, is paramount to the overall accuracy afforded by this modeling procedure. To this end, the required input parameters for wood, stucco, and gypsum walls were obtained either from the specialized computer program, CASHEW: Cyclic Analysis of Wood Shear Walls (Folz and Filiatrault, 2001), or from available experimental data (Isoda et al., 2001).

It must be noted that this simple modeling procedure is used to capture the global translational and torsional seismic response of light-frame wood buildings. With this simplified approach, the intent is not to model every connection between the various building elements. For example, roof-to-wall connections or anchor bolts are not explicitly modeled, as they are believed to be of secondary importance in the global seismic response of the structure. In addition, it is noted that this pancake modeling approach assumes only a shear deformation mode for the building over its height. Also, overturning effects are not accounted for in the modeling procedure. Nevertheless, this pancake modeling approach was shown to produce reasonably accurate global response predictions when compared against the results of shake table tests recently conducted on the full-scale two-story light-frame wood house shown in Figure 6 (Filiatrault et al., 2002).

Detailed information on the input parameters for the pancake models for each of the prototype index buildings considered in this study are given elsewhere (Isoda et al., 2001).

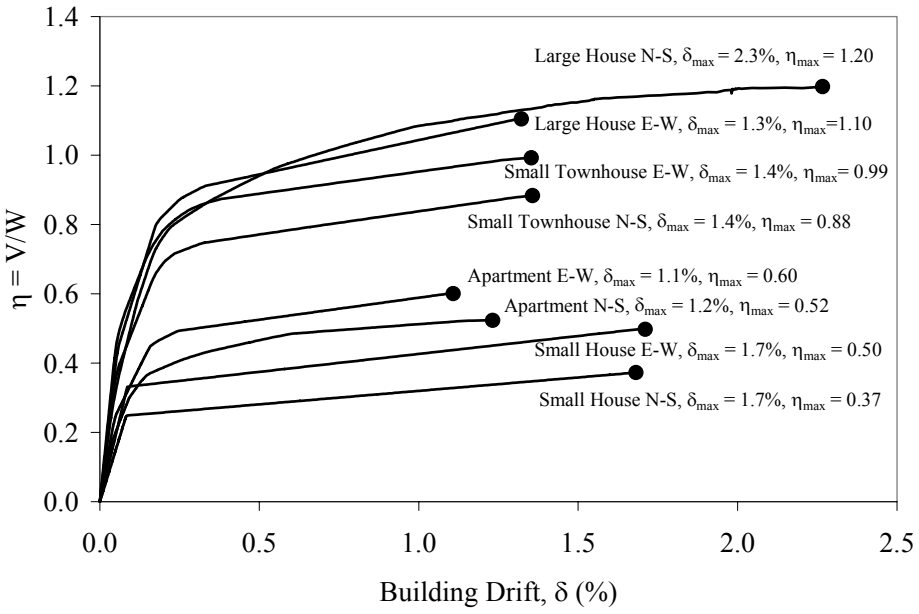

Fig. 8 Results of monotonic pushover analyses of index buildings

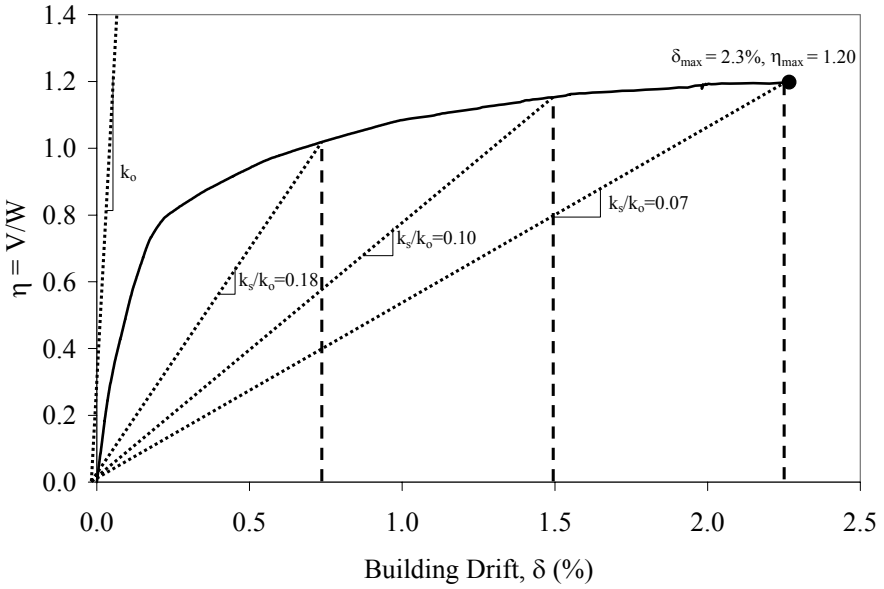

Fig. 9 Determination of secant stiffness at various drift levels, large house, N-S

Table 2: Secant Lateral Stiffness of the Index Buildings

Index Building	Direction	Initial Lateral Stiffness (kN/mm)	k_s/k_0		
			1/3 δ_{max}	2/3 δ_{max}	δ_{max}
Small House	East-West	22.6	0.18	0.10	0.08
	North-South	17.8	0.17	0.10	0.08
Large House	East-West	44.4	0.26	0.13	0.10
	North-South	40.5	0.18	0.10	0.07
Small Townhouse	East-West	139.0	0.18	0.11	0.08
	North-South	113.8	0.23	0.12	0.09
Apartment	East-West	100.2	0.23	0.14	0.10
	North-South	88.6	0.23	0.13	0.09

ANALYSIS PROCEDURE

The process of evaluating the appropriateness of the equivalent linear elastic modeling of wood buildings involved several different analyses of the prototype index buildings. In this section, the analysis procedure is briefly described along with a presentation of some specific results.

1. Monotonic Pushover Analyses

First, monotonic pushover analyses were performed in order to determine the envelope of the base shear – peak central roof displacement relationship for each of the index building. Lateral loads were applied in proportion to the weight distribution at each floor level and followed an inverse triangular distribution along the building height, typical of first mode response. The pushover analysis was carried out as a slow dynamic analysis using a gradual ramp loading function for each applied lateral load (Carr, 2000). The loads were applied slowly to ensure that inertia and viscous damping forces were minimal.

Figure 8 presents the results of the monotonic pushover analyses for all four index buildings along each of their orthogonal directions (north-south and east-west). The results are presented in non-dimensional terms: the normalized lateral load is a base shear coefficient, η, defined as the base shear divided by the seismic weight of each building (V/W), while the lateral displacement is expressed in terms of a building drift ratio, δ, defined as the lateral displacement at the center of the roof divided by the building height. The pushover curves in Figure 8 indicate that the maximum base shear coefficient, η_{max}, varies from 0.37 for the small house in the north-south direction to 1.20 for the large house in the north-

south direction. The building drift ratio, δ_{max}, corresponding to the maximum base shear coefficient varies from 1.1% for the apartment building in the east-west direction to 2.3% for the large house in the north-south direction.

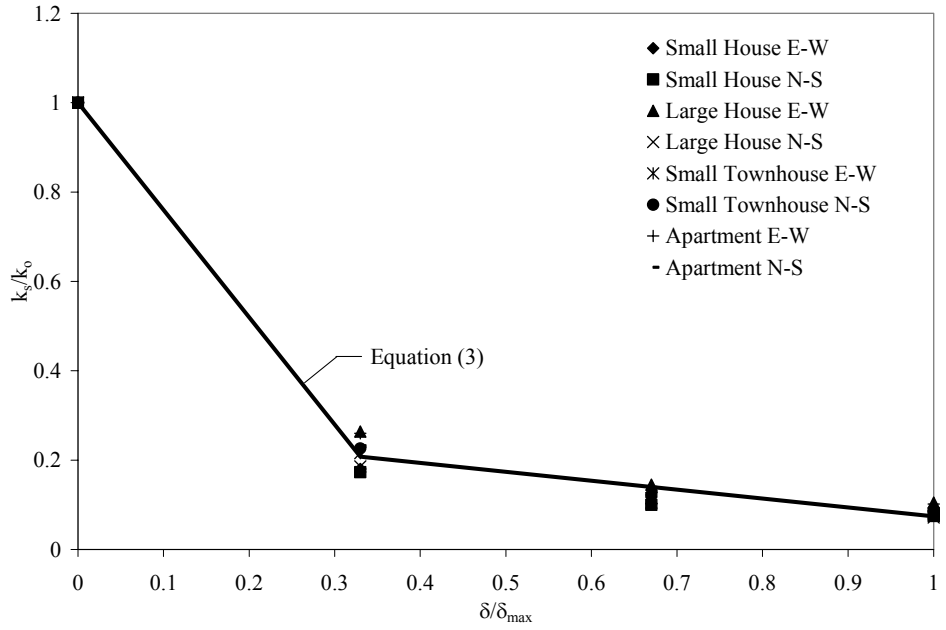

Fig. 10 Normalized secant lateral stiffness versus normalized drift levels for all index buildings

Using the normalized monotonic pushover curves shown in Figure 8, three drift levels were identified for evaluating the equivalent linear elastic modeling procedure. The first drift level corresponds to the drift ratio, δ_{max}, at maximum base shear coefficient, η_{max}, while the second and third correspond to 2/3 δ_{max} and 1/3 δ_{max}, respectively. For each drift level, the corresponding secant lateral stiffness, k_s, was computed, as illustrated in Figure 9, for the large house in the north-south direction. For each building model and drift level, the ratio k_s/k_o, where k_o is the initial lateral stiffness, was computed. The results of this analysis are presented in Table 2. The same results are displayed graphically in Figure 10. As shown in this figure, the variation of secant lateral stiffness with building drift ratio for all of the index buildings analyzed falls within a fairly narrow band. Consequently, this variation is not strongly dependent on the building configuration. Analytically, this variation can be represented adequately by two piece-wise linear segments, as follows:

$$\frac{k_s}{k_o} = \begin{cases} -2.4\dfrac{\delta}{\delta_{max}} + 1 & \text{for } \dfrac{\delta}{\delta_{max}} \le 0.33 \\ -0.2\left(\dfrac{\delta}{\delta_{max}} - 0.33\right) + 0.21 & \text{for } \dfrac{\delta}{\delta_{max}} > 0.33 \end{cases} \tag{3}$$

Assuming first mode response, Equation (3) can be transformed into a period variation equation:

$$\frac{T_s}{T_o} = \begin{cases} \dfrac{1}{\sqrt{-2.4\dfrac{\delta}{\delta_{max}} + 1}} & \text{for } \dfrac{\delta}{\delta_{max}} \le 0.33 \\ \dfrac{1}{\sqrt{-0.2\left(\dfrac{\delta}{\delta_{max}} - 0.33\right) + 0.21}} & \text{for } \dfrac{\delta}{\delta_{max}} > 0.33 \end{cases} \tag{4}$$

where T_s is the secant period corresponding to the target drift level, and T_o is the initial (elastic) fundamental period.

Referring again to Figure 8, it is noted that across the ensemble of monotonic pushover analyses of the index buildings, the mean building drift ratio, corresponding to the maximum base shear coefficient, is 1.5%. In a displacement-based design situation, this mean value for the building drift ratio along with an estimate of the initial fundamental period of the building could be used to estimate the secant period of vibration, through Equation (4), at a given target drift level.

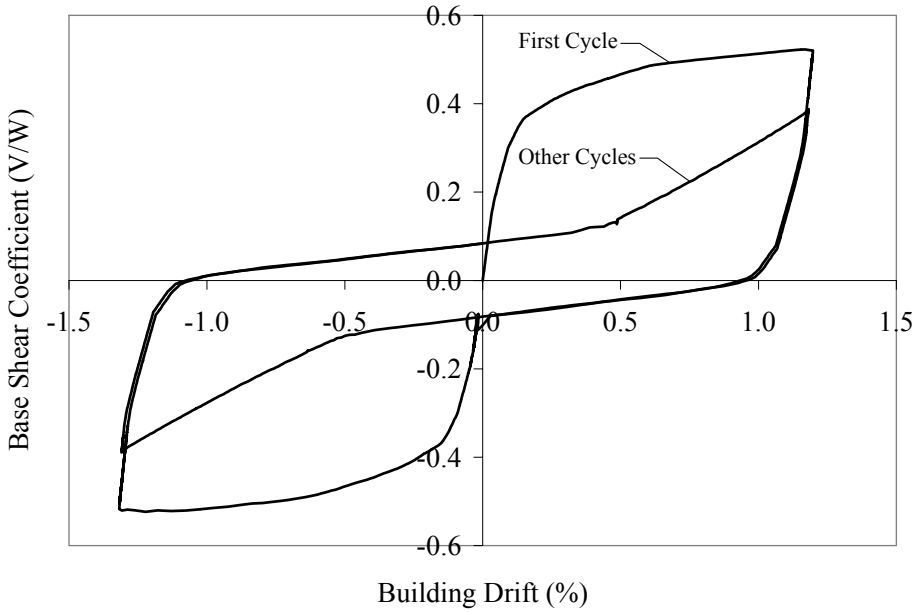

Fig. 11 Cyclic analysis: Apartment index building, north-south direction

Table 3: Equivalent Viscous Damping Ratios for the Index Buildings

Index Building	Direction of Loading	ζ_{eq}					
		1/3 δ_{max}		2/3 δ_{max}		δ_{max}	
		First Cycle	Other Cycles	First Cycle	Other Cycles	First Cycle	Other Cycles
Small House	East-West	0.30	0.18	0.29	0.19	0.28	0.17
	North-South	0.30	0.18	0.29	0.18	0.28	0.19
Large House	East-West	0.24	0.14	0.35	0.21	0.32	0.22
	North-South	0.26	0.16	0.30	0.18	0.25	0.15
Small Townhouse	East-West	0.39	0.23	0.30	0.18	0.27	0.16
	North-South	0.24	0.14	0.29	0.18	0.30	0.20
Apartment	East-West	0.31	0.18	0.26	0.16	0.29	0.19
	North-South	0.24	0.14	0.26	0.16	0.29	0.17

2. Cyclic Analyses

Following the monotonic pushover analyses described above, cyclic analyses were performed for each index building model and for each of the three drift levels considered. As a typical example, Figure 11 presents results of the cyclic analysis in the north-south direction for the apartment building at the drift level, δ_{max}, corresponding to the maximum base shear coefficient, η_{max}. Two full displacement cycles are considered in the cyclic analysis. This is done in order to capture the reduced energy dissipation after the first (virgin) cycle due to the stiffness degradation and pinching characteristics of the structure.

In order to capture the energy dissipation characteristics of each building configuration at a given building drift ratio, δ, an equivalent viscous damping ratio, ζ_{eq}, representative of the hysteretic damping in the structure, was computed from the global hysteretic behavior of each building configuration (Clough and Penzien, 1993):

$$\zeta_{eq} = \frac{E_{D\delta}}{2\pi\, k_s (\delta h)^2} \tag{5}$$

where $E_{D\delta}$ is the energy dissipated per cycle at the building drift ratio δ, k_s is the overall equivalent (secant) lateral stiffness of the building at the same drift level, and *h* is height of the building from the ground level to the roof eaves.

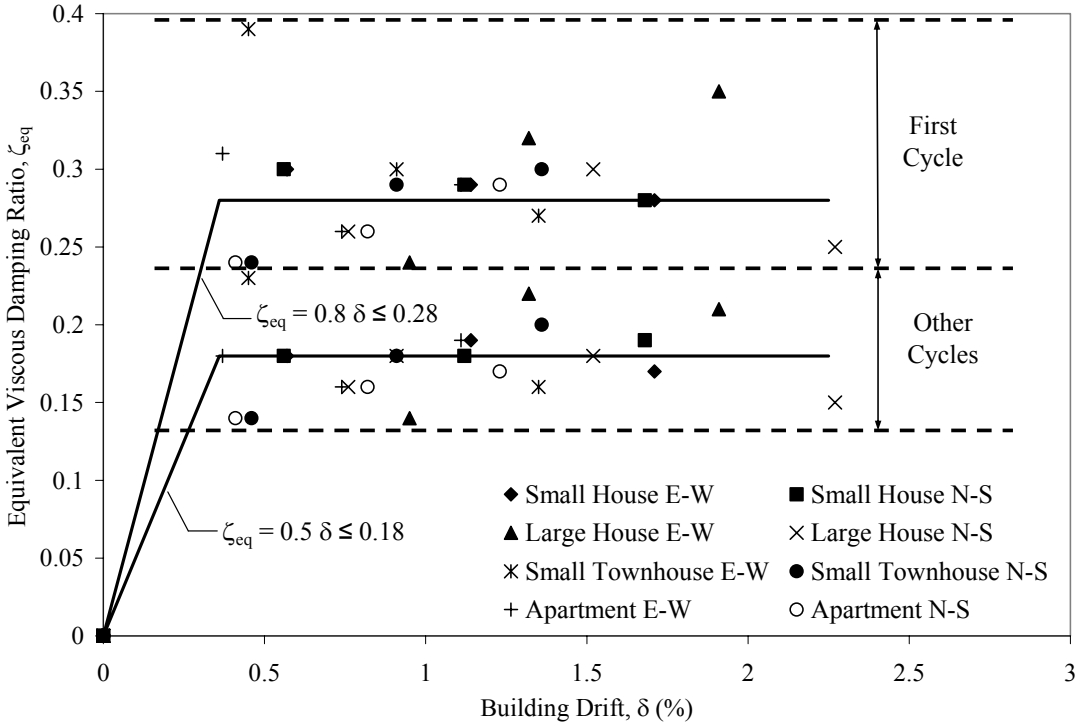

Fig. 12 Equivalent viscous damping ratios of index buildings

Equation (5) was applied twice to compute ζ_{eq}, once over the first hysteretic cycle, and then over the second cycle. The resulting values of ζ_{eq} for all index buildings and drift levels are listed in Table 3. The same results are displayed graphically in Figure 12. The equivalent damping ratios are significantly higher (in the vicinity of 30% of critical) for the first cycle calibration than for the second cycle calibration (in the vicinity of 20% of critical). Over the range of building drifts considered, the equivalent viscous damping ratio remains fairly constant with building drift ratio. Consequently, the variation of equivalent viscous damping ratio, ζ_{eq}, with building drift ratio, δ, can be represented reasonably accurately by the following empirical formulas:

$$\zeta_{eq} = \begin{cases} 0.8\delta & \text{for } \delta \le 0.35 \\ 0.28 & \text{for } \delta > 0.35 \end{cases} \tag{6}$$

for the first hysteretic cycle and

$$\zeta_{eq} = \begin{cases} 0.5\delta & \text{for } \delta \le 0.35 \\ 0.18 & \text{for } \delta > 0.35 \end{cases} \tag{7}$$

for all other cycles.

Note that the linear variation of ζ_{eq}, given in Equations (6) and (7), only applies for small values of building drift ratio (less than 0.35%). Numerical data, supporting this linear variation in ζ_{eq}, was established in a previous study (Filiatrault et al., 2003). This linear relationship is included in the specification of ζ_{eq}, since initial cracking of nonstructural wall finishes, such as gypsum wallboards and stucco, can occur at drift level less than 0.35% (Deierlein and Kanvinde, 2003). If cracking of nonstructural wall finishes is not part of the performance matrix, the constant values of ζ_{eq} specified in Equations (6) and (7) can be used.

Table 4: Characteristics of Earthquake Ground Motions (after Krawinkler et al., 2000)

Record Name	Earthquake Event	Year	Moment Magnitude	Station	Peak Acceleration (*g*)
CM2	Cape Mendocino	1992	7.1	Rio Dell Overpass-FF	0.39
LP1	Loma Prieta	1989	6.9	Capitola	0.53
LP2				Gilroy Array #3	0.55
LP3				Gilroy Array #4	0.42
LP5				Hollister Differential Array	0.28
LP6				Saratoga-W Valley College	0.33
NOR2	Northridge	1994	6.7	Beverly Hills 14145 Mulhol	0.42
NOR3				Canoga Park	0.36
NOR4				Glendale-Las Palmas	0.36
NOR9				North Hollywood Coldwater	0.27

Table 5: Scaling Factors for Earthquake Ground Motions

Index Building	Loading Direction	Drift Level	Scaling Factors									
			CM2	LP1	LP2	LP3	LP5	LP6	NOR2	NOR3	NOR4	NOR9
Small House	East West	$1/3\,\delta_{max}$	1.01	0.64	0.75	0.98	0.97	1.01	0.69	0.90	1.92	1.31
		$2/3\,\delta_{max}$	1.15	0.84	1.25	1.22	1.08	1.20	0.80	1.18	2.66	1.68
		δ_{max}	1.23	0.98	1.51	1.30	1.26	1.31	0.88	1.38	4.66	1.98
	North South	$1/3\,\delta_{max}$	0.73	0.51	0.75	0.74	0.73	0.78	0.52	0.80	1.58	1.12
		$2/3\,\delta_{max}$	0.89	0.73	1.01	0.94	0.86	0.94	0.60	1.00	2.80	1.48
		δ_{max}	1.04	0.87	1.21	1.07	1.14	1.03	0.69	1.14	4.70	1.68
Large House	East West	$1/3\,\delta_{max}$	1.80	0.97	1.38	1.91	2.18	2.06	1.41	1.57	1.97	2.22
		$2/3\,\delta_{max}$	2.42	1.62	2.26	2.57	2.39	2.62	1.67	2.44	4.50	3.25
		δ_{max}	2.69	1.92	2.69	2.84	2.49	2.82	1.86	2.88	5.55	3.74
	North South	$1/3\,\delta_{max}$	2.46	1.67	2.26	2.30	2.20	2.63	1.69	2.53	4.50	3.14
		$2/3\,\delta_{max}$	3.06	2.38	3.09	2.98	2.78	3.10	2.13	3.38	8.00	4.71
		δ_{max}	3.36	2.69	3.53	3.38	3.23	3.36	2.30	3.76	10.3	5.43
Small Townhouse	East West	$1/3\,\delta_{max}$	2.18	1.08	1.53	2.02	2.23	2.25	1.52	1.78	2.59	2.51
		$2/3\,\delta_{max}$	2.45	1.40	1.88	2.30	2.36	2.53	1.70	2.07	4.27	2.94
		δ_{max}	2.62	1.72	2.43	2.70	2.44	2.69	1.85	2.48	5.12	3.57
	North South	$1/3\,\delta_{max}$	1.68	0.84	1.18	1.65	1.81	1.83	1.21	1.43	1.86	1.92
		$2/3\,\delta_{max}$	1.90	1.29	1.91	2.03	1.92	2.23	1.45	2.01	4.00	2.61
		δ_{max}	2.20	1.62	2.32	2.35	2.09	2.39	1.62	2.28	5.06	3.39
Apartment	East West	$1/3\,\delta_{max}$	1.37	0.82	1.15	1.08	1.15	1.34	0.88	1.22	2.54	1.67
		$2/3\,\delta_{max}$	1.58	1.18	1.54	1.39	1.32	1.52	1.05	1.52	3.85	2.37
		δ_{max}	1.85	1.46	2.20	1.68	1.66	1.74	1.17	1.92	7.50	2.71
	North South	$1/3\,\delta_{max}$	1.14	0.85	1.00	0.96	1.02	1.16	0.81	1.28	2.56	1.66
		$2/3\,\delta_{max}$	1.39	1.21	1.66	1.39	1.40	1.48	0.97	1.67	4.73	2.40
		δ_{max}	1.66	1.52	2.42	1.92	1.95	1.69	1.17	.93	7.70	2.78

3. Dynamic Analyses

Following the monotonic pushover and cyclic analyses described above, time-history dynamic analyses were performed on the index buildings under an ensemble of 10 historical strong ground motion records from three different California earthquakes. These records are representative of ordinary

earthquakes having a probability of exceedance of 10% in 50 years (Krawinkler et al., 2000). These records are free of any forward directivity effects (near-fault effects). All ground motions were recorded on soil types C or D, and were generated by earthquakes of moment magnitude, M_w, ranging from 6.7 to 7.3. The hypocentral distance for these records range between 13 and 25 km. Table 4 lists these earthquake records along with other pertinent details on their characteristics.

Non-linear time-history dynamic analyses were first conducted on the index building models under each of the unscaled ground motion records. The energy dissipation capacity of these structures was considered mainly through hysteretic damping of the various structural elements: wood, gypsum, and stucco walls, each modeled with the Wayne Stewart hysteretic rule. In addition, a nominal viscous damping ratio of 1% of critical was introduced in the first two elastic modes of these building models. Further details of these models are presented elsewhere (Isoda et al., 2001).

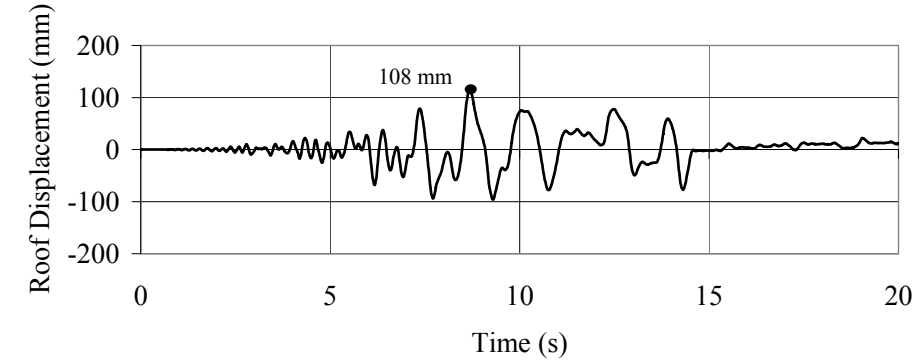

a) Non-linear Building Model

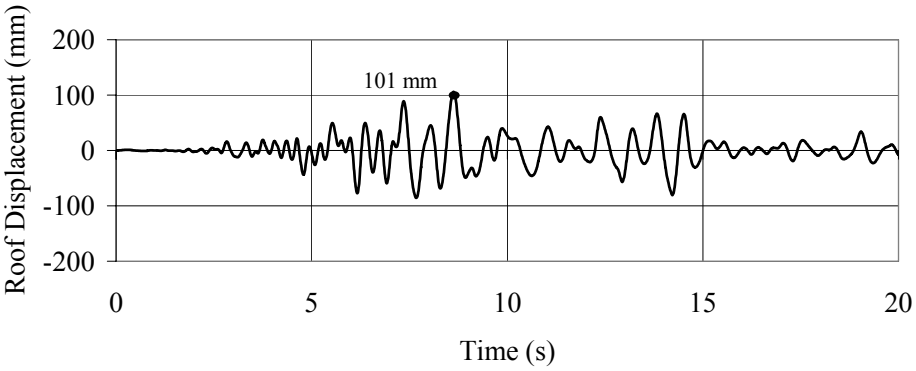

b) Linear Model with Damping from First Hysteretic Cycle

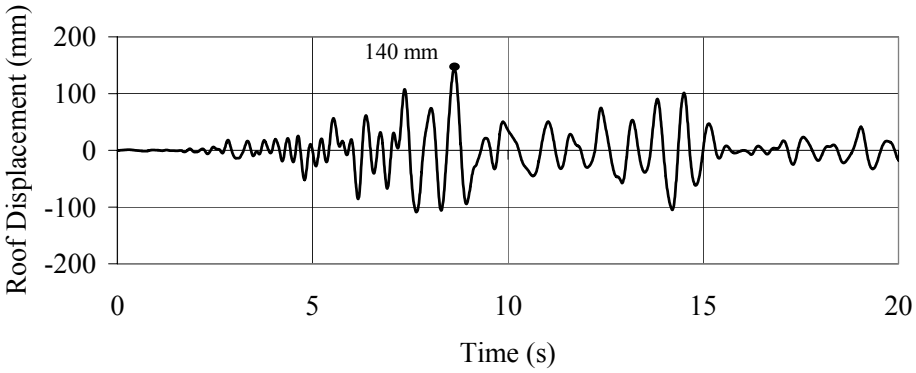

c) Linear Model with Damping from Other Hysteretic Cycles

Fig. 13 Roof relative displacement time-histories for the large house index building under LP1 record scaled to δ_{max}

An iterative procedure was then used to scale the peak ground acceleration (PGA) of each earthquake record such that the peak displacement at the top of each building model matched the three specified drift levels: $1/3\,\delta_{\max}$, $2/3\,\delta_{\max}$, and $\delta_{\max}$. This procedure was undertaken for the two excitation directions of each index building. The resulting scaling factors obtained from this exercise are given in Table 5.

Equivalent linear-elastic models of the index buildings were then established and analyzed, using the computer program RUAUMOKO, under the ensemble of ground motions, scaled according to Table 5 for the two excitation directions and three drift levels. The linear building models were obtained from the non-linear models by first replacing all of non-linear shear wall spring elements (which obeyed the Wayne Stewart hysteretic rule) with linear elastic spring elements. Following this, the initial lateral stiffness of each structural element in each building model was multiplied by the stiffness ratios k_s/k_o given in Table 2. The damping ratios in the first two elastic modes of the building models were then adjusted according to the damping ratios given in Table 4. This linearization procedure allowed for a direct comparison between the predictions of equivalent linear elastic (secant) models and those of the full non-linear building models.

As an initial example of this procedure, Figure 13 shows the relative displacement time-history predictions at the center of the roof for the large house index building, excited in the north-south direction by the LP1 record scaled to the drift level, $\delta_{\max}$, using the non-linear model and the equivalent linear model, using the two values of equivalent viscous damping ratios, ζ_{eq}, specified in Table 4. In this particular case, the maximum roof displacement predicted by the linear model is 7% below that predicted by the full non-linear model for ζ_{eq} based on the first (virgin) hysteretic cycle and 30% above the non-linear model when ζ_{eq} is based on all other hysteretic cycles.

The comparative analysis that follows is between the non-linear models and the equivalent linear models of the index buildings, each represented as multi-degree-of-freedom systems. In a displacement-based seismic design approach, the structural system will need to be reduced further to a linear single-degree-of-freedom system. This model reduction step was not performed here in order that the validity of the proposed equivalent modeling procedure could be properly evaluated.

ANALYSIS RESULTS

In order to properly quantify the accuracy of the equivalent linear models in relation to the corresponding non-linear models, three different measures of time-history response were considered in this study.

The first response parameter considered is the peak displacement ratio, PDR, defined as:

$$\text{PDR} = \frac{\text{Peak Roof Displacement of Linear Model}}{\text{Peak Roof Displacement of Non-linear Model}} \tag{8}$$

This parameter is used to assess how well the equivalent linear models are able to reproduce the peak seismic response of the fully non-linear models. Note that this is the only response parameter considered in the direct-displacement seismic design procedure.

The second response parameter considered is the RMS displacement ratio, RMSDR, defined as:

$$\text{RMSDR} = \frac{\text{Root Mean Square Roof Displacement of Linear Model}}{\text{Root Mean Square Displacement Non-linear Model}} \tag{9}$$

This parameter is used to assess how well the equivalent linear models are able to reproduce, in an average sense, the displacement response time-history of the fully non-linear models.

Finally, the third response parameter considered is the input energy ratio, IER, defined as:

$$\text{IER} = \frac{\text{Final Seismic Input Energy of Linear Model}}{\text{Final Seismic Input Energy of Non-linear Model}} \tag{10}$$

This parameter is used to assess how well the equivalent linear models are able to reproduce the seismic energy transmitted to the fully non-linear models.

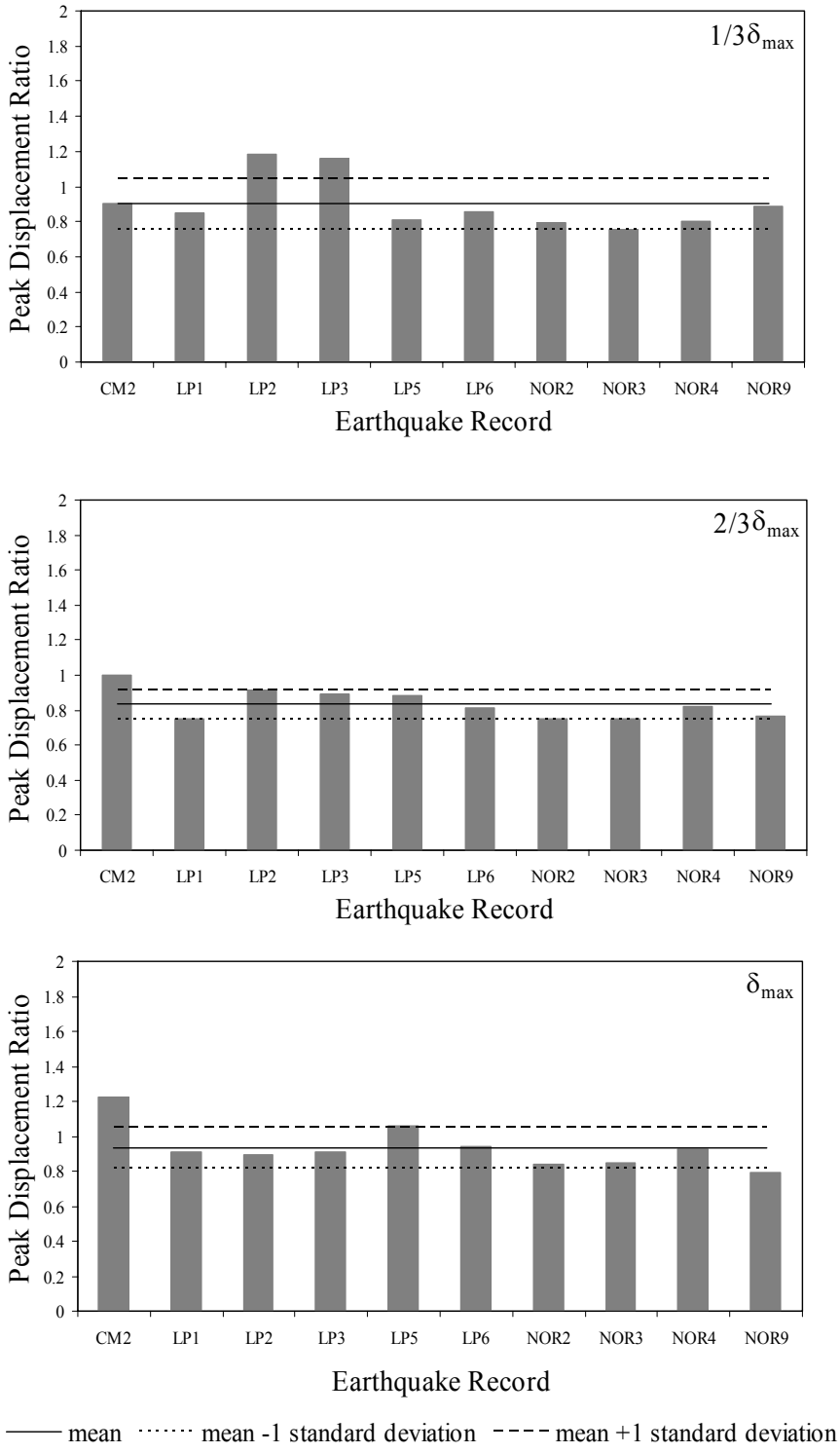

Fig. 14 Peak displacement ratios, large house, north-south, first cycle hystereses

1. Results for Large House in North-South Direction

In this study, detailed comparative analyses of the large house in the north-south direction were first undertaken. A summary of the results follows.

Figures 14 and 15 show the PDR values obtained for the large house along its north-south direction under the ensemble of earthquake records, three drift levels, and for the linear models based on the first and all other hysteretic response cycles, respectively. Also presented in these figures are mean and mean ± 1 standard deviation (std. dev.) PDR values across the earthquake ensemble. As shown in Figure 14 for the linear model based on the first hysteretic cycle, the mean PDR value is slightly less (−10%) than unity

for the three drift levels considered, thereby indicating that the mean peak roof displacement of the linear model slightly under-predicts the mean peak roof displacement of the fully non-linear model. The mean + 1 std. dev. value of the PDR, however, is slightly higher (+10%) than unity for drift levels corresponding to 1/3 δ_{max} and δ_{max}, but is slighter lower (−5%) than unity for a drift level corresponding to 2/3 δ_{max}. The results of Figure 15 for the linear model based on all other hysteretic cycles indicate, on the other hand, that this linear model over-predicts (+20% for mean and +40% for mean + 1 std. dev.) the peak roof displacement of the fully non-linear building models for all three drift levels considered.

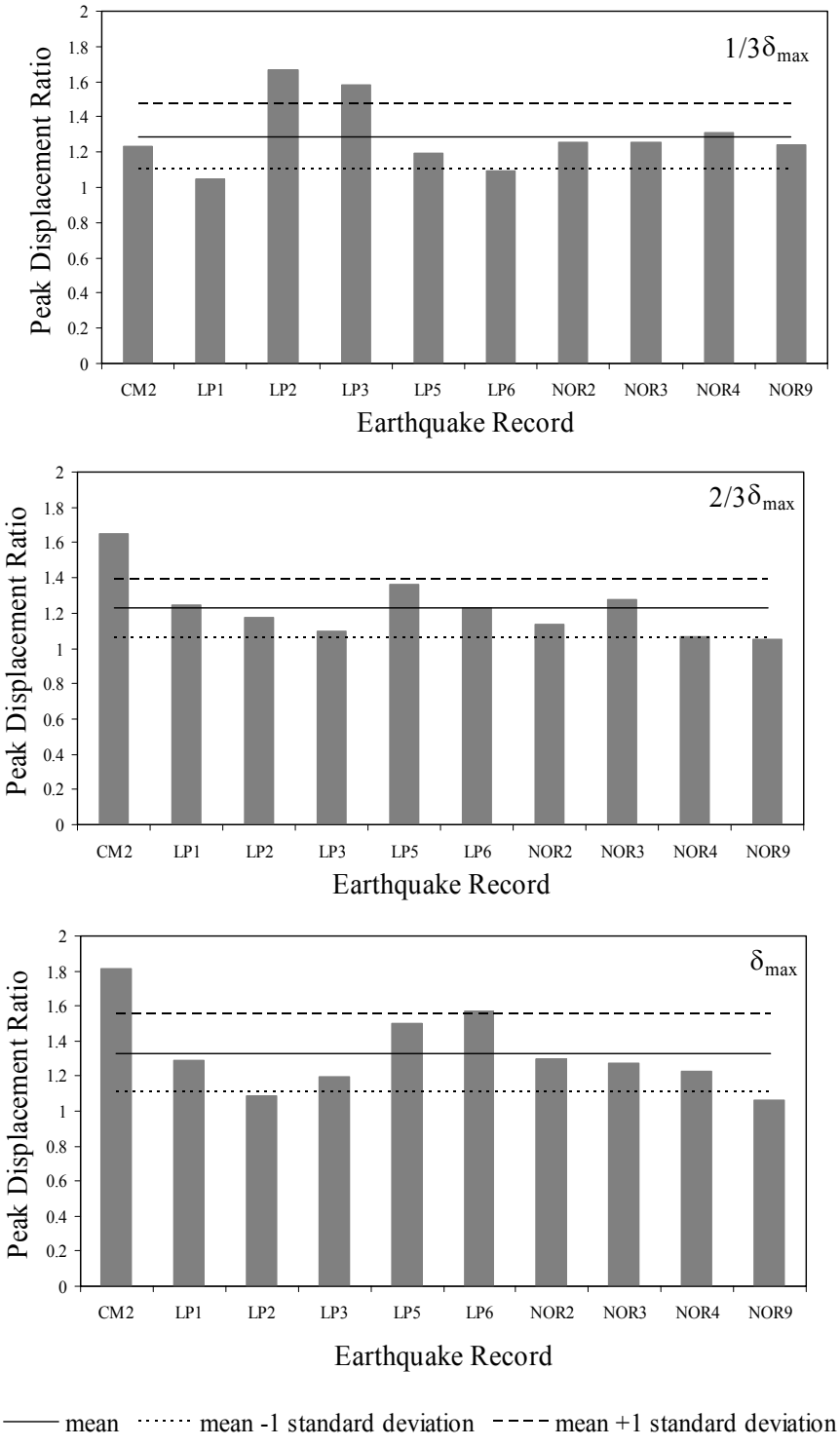

Fig. 15 Peak displacement ratios, large house, north-south, other cycles hystereses

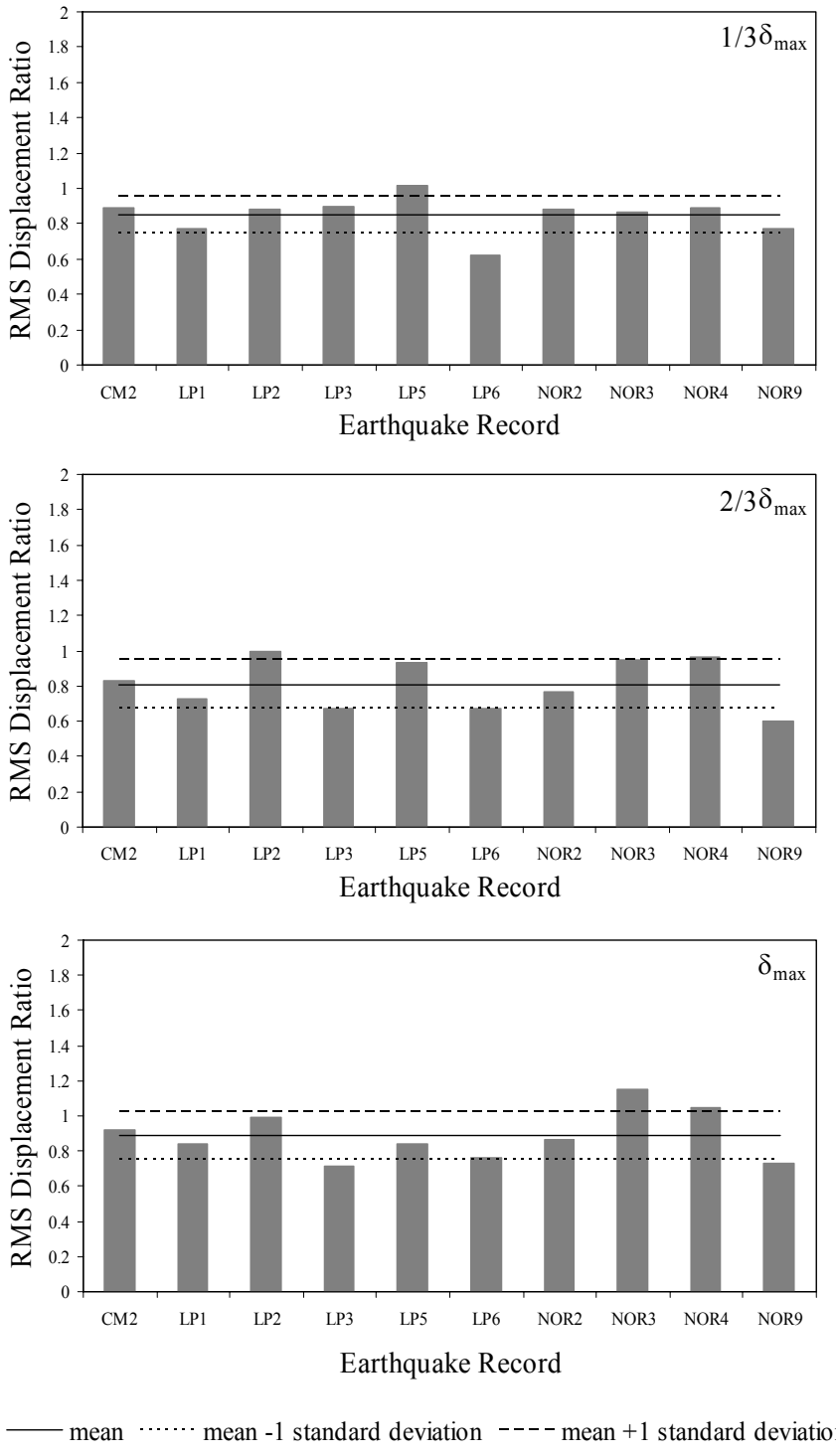

Fig. 16 RMS displacement ratios, large house, north-south, first cycle hystereses

Figures 16 and 17 present the RMSDR values obtained for the large house along its north-south direction under all earthquake records, three drift levels, and for the linear models based on the first and all other hysteretic response cycles, respectively. The results obtained are very similar to those obtained previously with the linear model based on the first hysteretic cycle slightly under-predicting (−10% for mean) the RMS response of the fully non-linear model. Similarly, the linear model based on all other hysteretic cycles over-predicts (+30% for mean and +50% for mean + 1 std. dev.) the mean RMS response of the fully non-linear model.

Figures 18 and 19 present the IER values obtained for the large house along its north-south direction under all earthquake records, three drift levels, and for the linear models based on the first and all other hysteretic response cycles, respectively. In this case, both first and other cycles linear models over-predict the input energy to the fully non-linear model.

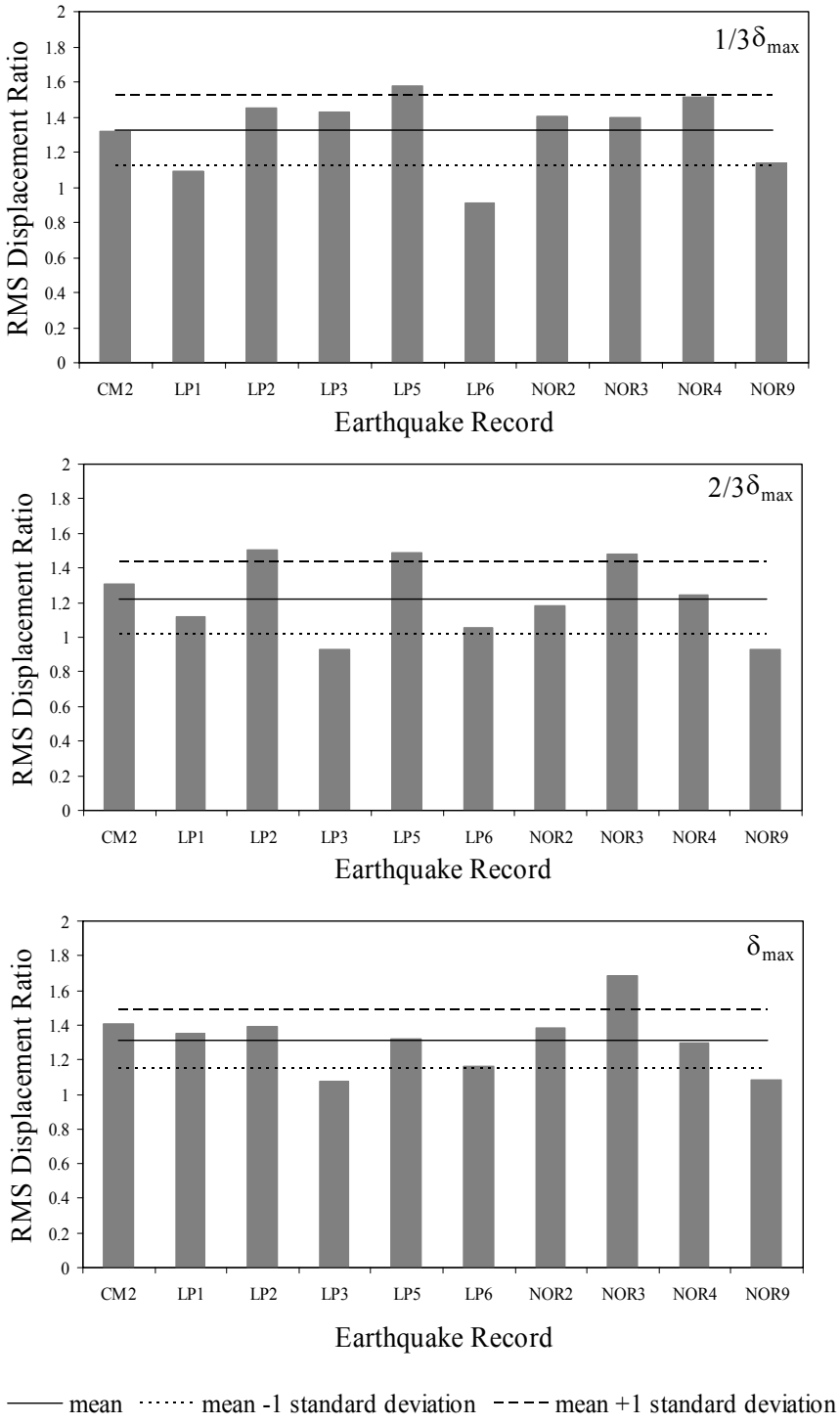

Fig. 17 RMS displacement ratios, large house, north-south, other cycles hystereses

2. Results for Other Index Buildings

For the analyses of the other index buildings, only the peak displacement ratio (PDR) was considered. Also, only the linear models based on the first hysteretic cycle were investigated.

Figure 20 presents, for all index buildings and directions, the mean and mean ± 1 std. dev. values of the peak displacement ratio, PDR, taken across the earthquake ensemble. The results are similar for all building types and directions with the linear elastic models under-predicting by 20% on average the mean value of the PDR.

Figure 21 presents the variation of the mean value of the PDR with building drift ratio for all index buildings and drift levels. These results indicate that the mean value of the PDR is relatively insensitive

to the drift level and building type. The mean PDR varies around 0.80 indicating that the elastic models based on first cycle hysteretic response under-predicts the peak displacement response of the fully non-linear models by 20% on average.

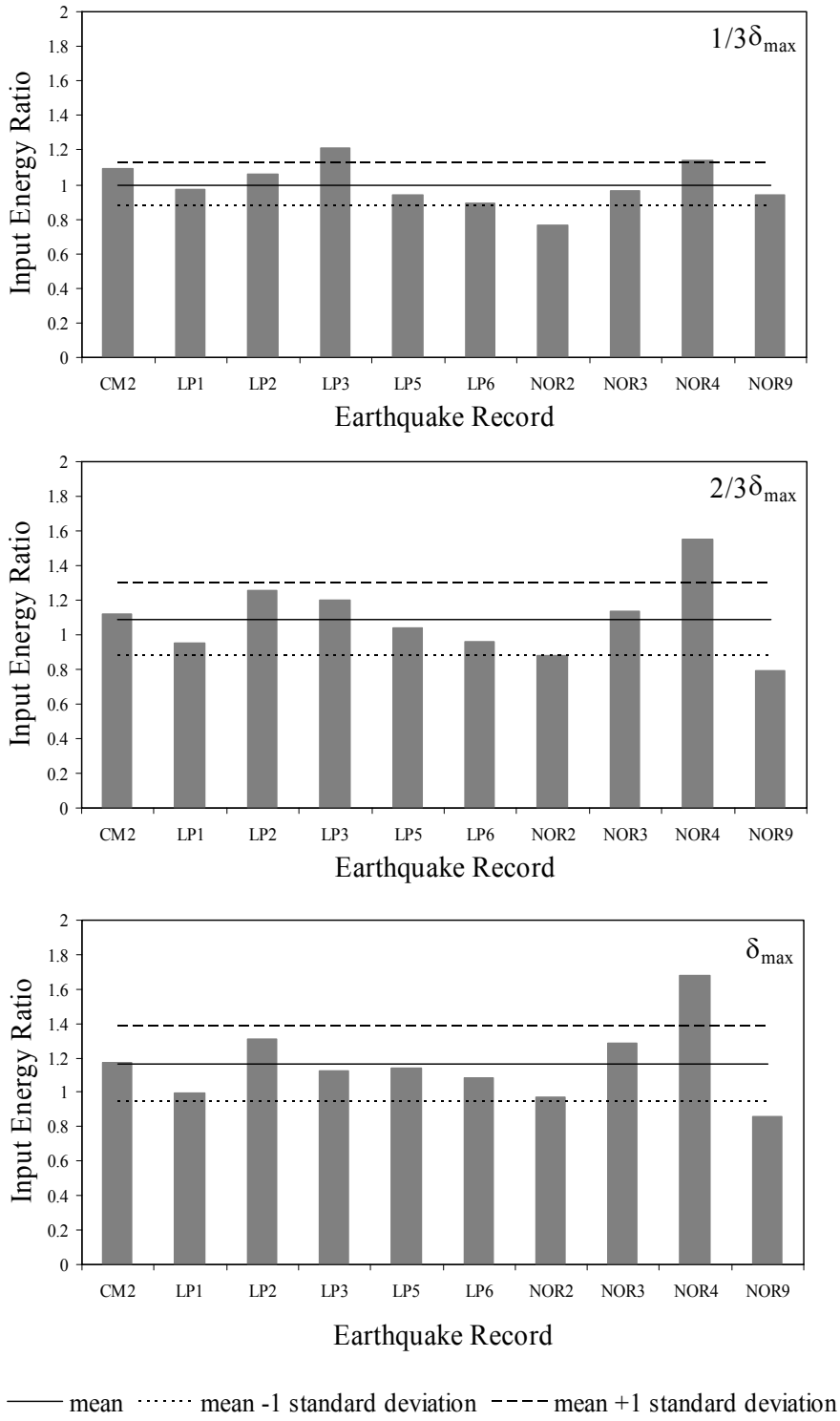

Fig. 18 Input energy ratios, large house, north-south, first cycle hystereses

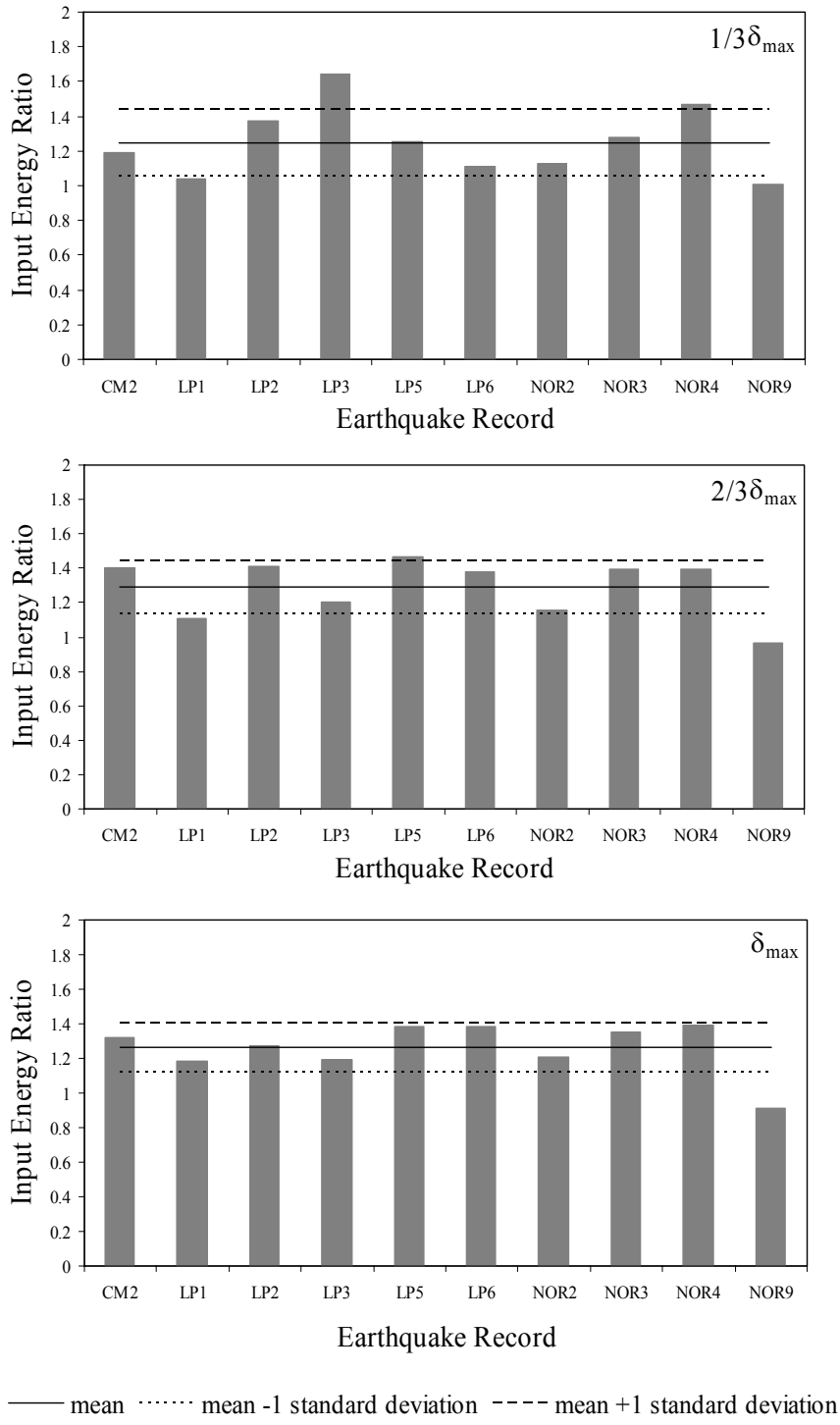

Fig. 19 Input energy ratios, large house, north-south, other cycles hystereses

DISCUSSION

The numerical results, presented in the previous sections, indicate that modeling the seismic response of a light-frame wood building with an equivalent linear model using a damping ratio associated with energy dissipation in the first (virgin) hysteretic response under-predicts its peak displacement by 20% on average. From the results obtained in this study, this under-prediction is relatively insensitive to the drift level and building type.

One approach to take this under-prediction into account in the displacement-based design of a light-frame wood building would be to associate the target displacement, Δ_t, with a linear-elastic system based on a displacement equal to 80% of Δ_t. In this case, the equivalent elastic period of the building, T_{eq},

would be obtained from the design displacement response spectrum at a spectral displacement equal to $0.80\,\Delta_t$ and for a damping ratio obtained from the virgin hysteretic response, as expressed by Equation (6). The displacement-based design process would then proceed as outlined, but with a target displacement equal to $0.80\,\Delta_t$. While this approach is simple, it suffers from having to adjust the target displacement Δ_t, which is the key parameter in the displacement-based design methodology and is intimately tied to the specified seismic hazard level.

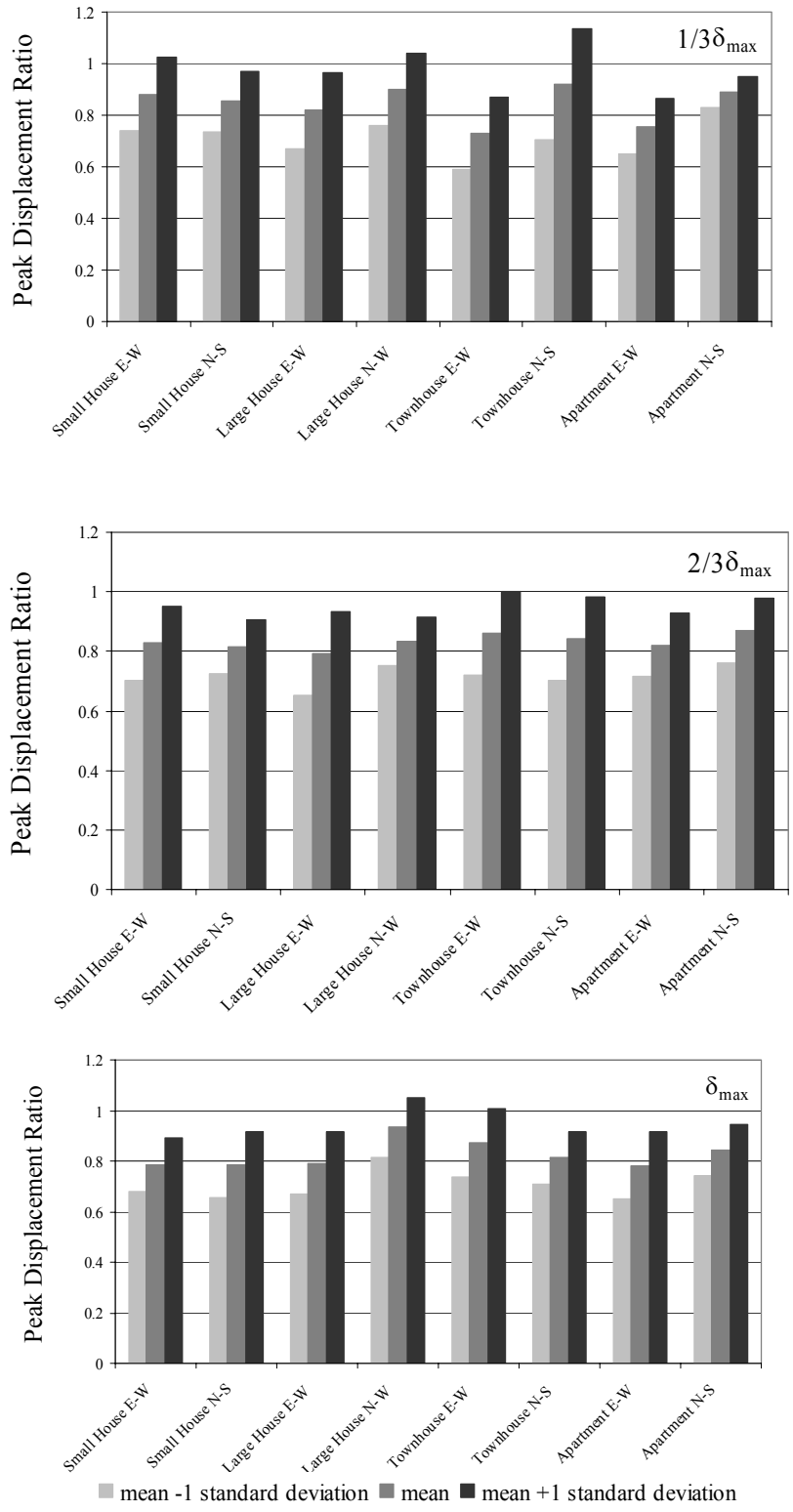

Fig. 20 Peak displacement ratios for all index buildings and directions

Another approach would be to use Δ_t as the target displacement in concert with a design displacement response spectrum at a damping value representative of the cyclic response of the building after the first full cycle, as expressed by Equation (7). This approach is more conservative, since the final equivalent elastic model would actually over-predict the displacement of the non-linear model, as shown by the numerical results obtained herein.

Alternatively, one could use a weighted damping ratio that is bounded by the values corresponding to the first and the other cyclic response. This weighted damping ratio would, in part, be ground motion dependent: requiring a heavier weight to first cycle hysteretic response for pulse motions and vice-versa for long subduction-zone motions. The determination of the appropriate damping weighting factors would require an iterative analysis procedure, which would be computationally intensive. Further studies are required to determine if this level of refinement is worth pursuing.

Finally, it is noted that further research is also required to evaluate the consequence of reducing the equivalent linear elastic building models, described herein, to single-degree-of-freedom systems as part of the proposed displacement-based design procedure.

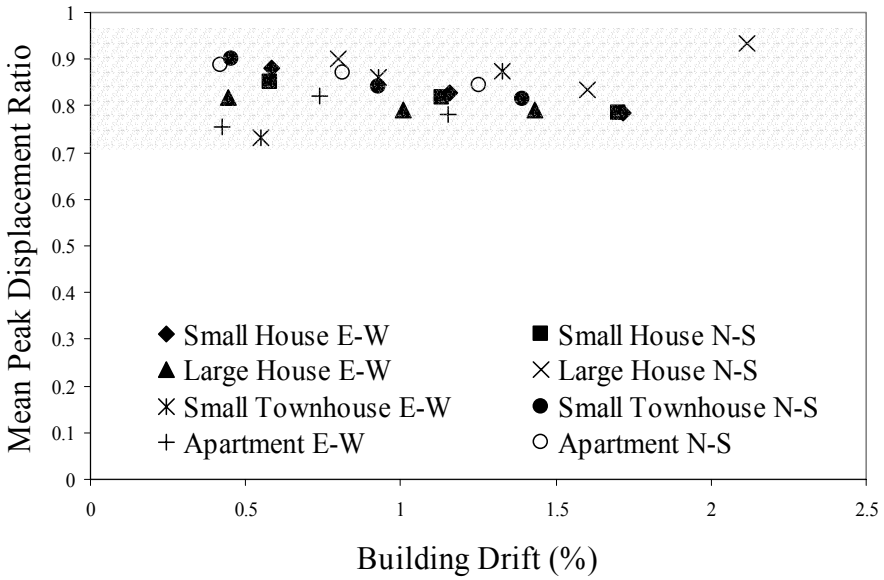

Fig. 21 Variation of mean peak displacement ratio with building drift ratio

CONCLUSIONS

This paper has presented the results from an extensive numerical investigation into the appropriateness of equivalent linear elastic modeling of light-frame wood buildings in the context of a direct-displacement based design approach. The numerical results obtained along two orthogonal directions of four light-frame wood prototype index buildings excited by an ensemble of 10 different historical earthquake records causing three different levels of building drift response indicate that elastic models based on an equivalent viscous damping representative of hysteretic response of the first (virgin) cycle under-predict by 20% on average the seismic response of the corresponding non-linear models. On the other hand, elastic models based on an equivalent viscous damping representative of the second cycle of the hysteretic response over-predict significantly (40% on average) the seismic response of fully non-linear models. Various approaches have been briefly presented to show how the response differences between equivalent linear elastic and fully inelastic building models can be taken into account in the direct-displacement based design process. In turn, this has highlighted the need for future research aimed at refining the displacement-based seismic design procedure for light-frame wood buildings.

REFERENCES

1. Carr, A.J. (2000). "RUAUMOKO – Inelastic Dynamic Analysis Program", Department of Civil Engineering, University of Canterbury, Christchurch, New Zealand.

2. Clough, R.W. and Penzien, J. (1993). "Dynamics of Structures", Second Edition, McGraw Hill, New York, U.S.A.
3. Deierlein, G. and Kanvinde, A. (2003). "Seismic Performance of Gypsum Walls – Analytical Investigation", Report W-23, Consortium of Universities for Earthquake Engineering (CUREE), Richmond, CA, U.S.A.
4. Filiatrault, A. and Folz, B. (2002). "Performance-Based Seismic Design of Wood Framed Buildings", ASCE Journal of Structural Engineering, Vol. 128, No. 1, pp. 39-47.
5. Filiatrault, A., Fischer, D., Folz, B. and Uang, C.-M. (2002). "Seismic Testing of a Two-Story Woodframe House: Influence of Wall Finish Materials", ASCE Journal of Structural Engineering, Vol. 128, No. 10, pp. 1337-1345.
6. Filiatrault, A., Isoda, H. and Folz, B. (2003). "Hysteretic Damping of Wood Framed Buildings", Engineering Structures, Vol. 25, No. 4, pp. 461-471.
7. Foliente, G.C. (1995). "Hysteresis Modeling of Wood Joints and Structural Systems", ASCE Journal of Structural Engineering, Vol. 121, No. 6, pp. 1013-1022.
8. Folz, B. and Filiatrault, A. (2001). "Cyclic Analysis of Wood Shear Walls", ASCE Journal of Structural Engineering, Vol. 127, No. 4, pp. 433-441.
9. Isoda, H., Folz, B. and Filiatrault, A. (2001). "Seismic Modeling of Index Woodframe Buildings", Report W-12, Consortium of Universities for Research in Earthquake Engineering (CUREE), Richmond, CA, U.S.A.
10. Krawinkler, H., Parisi, F., Ibarra, L., Ayoub, A. and Medina, A.R. (2000). "Development of a Testing Protocol for Wood Frame Structures", Report W-02, Consortium of Universities for Research in Earthquake Engineering (CUREE), Richmond, CA, U.S.A.
11. Porter, K.A., Beck, J.L., Seligson, H.A., Scawthorn, C.R., Tobin, L.T., Young, R. and Boyd, T. (2001). "Improving Loss Estimation for Woodframe Buildings", Report W-18, Consortium of Universities for Research in Earthquake Engineering (CUREE), Richmond, CA, U.S.A.
12. Priestley, M.J.N. (1993). "Myths and Fallacies in Earthquake Engineering – Conflicts between Design and Reality", Bulletin of the New Zealand National Society for Earthquake Engineering, Vol. 26, No. 3, pp. 329-341.
13. Priestley, M.J.N. (1998). "Displacement-Based Approaches to Rational Limit States Design of New Structures", Proceedings of 11th European Conference on Earthquake Engineering, Paris, France, Keynote Address.
14. Reitherman, R., Cobeen, K. and Serban, K. (2003). "Design Documentation of Woodframe Project Index Buildings", Report W-29, Consortium of Universities for Research in Earthquake Engineering (CUREE), Richmond, CA, U.S.A.
15. Stewart, W.G. (1987). "The Seismic Design of Plywood Sheathed Shear Walls", Ph.D. Thesis, University of Canterbury, Christchurch, New Zealand.